

Gas-phase electrochemistry: Measuring absolute potentials and investigating ion and electron hydration*

William A. Donald^{1,‡} and Evan R. Williams²

¹*School of Chemistry, Bio21 Institute of Molecular Science and Biotechnology, and ARC Centre of Excellence for Free Radical Chemistry and Biotechnology, University of Melbourne, Melbourne, Victoria, Australia;* ²*Department of Chemistry, University of California, Berkeley, CA, USA*

Abstract: In solution, half-cell potentials and ion solvation energies (or enthalpies) are measured relative to other values, thus establishing ladders of thermochemical values that are referenced to the potential of the standard hydrogen electrode (SHE) and the proton hydration energy (or enthalpy), respectively, which are both arbitrarily assigned a value of 0. In this focused review article, we describe three routes for obtaining absolute solution-phase half-cell potentials using ion nanocalorimetry, in which the energy resulting from electron capture (EC) by large hydrated ions in the gas phase are obtained from the number of water molecules lost from the reduced precursor cluster, which was developed by the Williams group at the University of California, Berkeley. Recent ion nanocalorimetry methods for investigating ion and electron hydration and for obtaining the absolute hydration enthalpy of the electron are discussed. From these methods, an absolute electrochemical scale and ion solvation scale can be established from experimental measurements without any models.

Keywords: absolute potentials; clusters; electrochemistry; electron capture dissociation; electron transfer; gaseous state; hydrated ions; hydration; ion nanocalorimetry; solvation; thermochemistry.

INTRODUCTION

The solvation of ions, such as protons [1,2] or excess electrons in liquid water [3,4], remains interesting because of the important role that ion–solvent interactions play in chemical transformations involving charge transfer and neutralization. Ions can undergo a number of important inter- and intra-molecular processes in solution, such as ion–ion association, electron- or proton-transfer reactions, and/or conformational changes, all of which are affected by ion–solvent interactions and the degree to which the ion is stabilized by such interactions. One of the best ways to characterize ion–solvent interactions is to determine the absolute energy and enthalpy of transferring an ion that is isolated in the gas phase with no kinetic energy into the bulk of the solvent of interest that is, ideally, independent of any counterions, i.e., to determine absolute ion solvation energy and enthalpy values. Despite extensive efforts devoted to obtaining these values, absolute ion solvation enthalpies and energies have not been measured directly. In contrast, the corresponding relative values, in which the relative thermodynamic con-

Pure Appl. Chem.* **83, 2115–2212 (2011). A collection of invited, peer-reviewed articles by the winners of the 2011 IUPAC Prize for Young Chemists.

[‡]Corresponding author: E-mail: wdonald@unimelb.edu.au

tribution of a single ion is referenced to that of another ion, can be measured accurately using calorimetric and/or electrochemical methods [5,6]. These relative values are commonly referenced to the value for the proton, for which the relative solvation energy or enthalpy is arbitrarily assigned a value of 0. Therefore, if the absolute ion solvation energy or enthalpy value for just a single ion can be obtained, then the entire ion solvation scale can be converted to an absolute scale.

Another way to separate the thermodynamic contribution of a single ion from counterions would be to determine the absolute electrochemical potential of a single half-cell reaction, which can be used to obtain absolute solvation energies using thermodynamic cycles and known thermochemical data (*vide infra*). However, in solution, the potentials of half-cell reactions are measured relative to other half-cells, thus resulting in a ladder of thermochemical values that is anchored to the standard hydrogen electrode (SHE), $\text{H}^+(\text{aq}) + \text{e}^- \rightarrow \frac{1}{2}\text{H}_2(\text{g})$, which is arbitrarily assigned a value of 0 V. If the potential of a single absolute half-cell potential is obtained in isolation from another, an absolute electrochemical scale can be established. An absolute scale is important for determining the band structure of water [1] and for evaluating the accuracy of ion solvation models [7,8], which are used extensively for studying the structure, dynamics, and reactivity of ions in solution using computational methods [9,10]. As a result of the importance of establishing absolute electrochemical and ion solvation thermodynamic scales, extensive effort and enthusiasm has been directed toward measuring absolute potentials for single half-cells in isolation [11–21]. However, this topic remains controversial largely because the many approaches for obtaining absolute potentials are indirect and a relatively wide range of values have been reported for the absolute SHE potential.

One definition for the absolute SHE potential is the potential of the SHE reaction referenced to an electron at infinite distance [11,12]. From a simple thermodynamic cycle, the standard absolute Gibbs free energy of the SHE reaction is given by eq. 1

$$\Delta G_{\text{abs}}(\text{SHE}) = -\alpha_{\text{aq}}(\text{H}^+) - \Delta G_{\text{at}}(\frac{1}{2}\text{H}_2) - \Delta G_{\text{ion}}(\text{H}) \quad (1)$$

where $\alpha_{\text{aq}}(\text{H}^+)$ is the standard “real” hydration free energy of the proton, which is given by the sum of the standard absolute proton hydration Gibbs free energy, $\Delta G_{\text{aq}}(\text{H}^+)$, and the surface potential of water that results from the orientation of water molecules at the gas–water interface. $\Delta G_{\text{at}}(\frac{1}{2}\text{H}_2)$ and $\Delta G_{\text{ion}}(\text{H})$ are the standard Gibbs free energy for the atomization and ionization of $\frac{1}{2}\text{H}_2$ and H, respectively. $\Delta G_{\text{abs}}(\text{SHE})$ can be readily converted to the absolute SHE potential, $E_{\text{abs}}(\text{SHE})$, using the Faraday equation ($E = -nF\Delta G$, where F is the Faraday constant and n is the number of electrons transferred in the reaction). An alternative definition is to not include the surface potential of water, and substitute $\alpha_{\text{aq}}(\text{H}^+)$ in eq. 1 for the absolute proton hydration Gibbs free energy, $\Delta G_{\text{aq}}(\text{H}^+)$ [7].

As a result of the thermodynamic cycle represented by eq. 1, if a value for the absolute or real hydration energy of the proton is obtained, then a value for the absolute SHE potential can be obtained [7,11]. Values for the absolute SHE potential obtained using values for either $\alpha_{\text{aq}}(\text{H}^+)$ or $\Delta G_{\text{aq}}(\text{H}^+)$ differ by the surface potential of water, which has not been directly measured, but is believed to be small in magnitude [22,23]. Values for absolute or real proton hydration energies have been obtained from high-resistance voltaic-cell electrochemical measurements [11,12,24], cluster measurements [7,25–30], and by computational methods [31–33]. The 1986 IUPAC-recommended value for the absolute SHE potential is +4.44 V [11], which was obtained using a value of –260.0 kcal/mol for $\alpha_{\text{aq}}(\text{H}^+)$, which was reported by Farrell and McTigue [24]. This value was obtained by extrapolating high-resistance voltaic-cell potential measurements between a streaming mercury electrode and a streaming aqueous hydrochloric acid solution to infinite HCl dilution using a model [34] that relates the difference in the surface potential between the HCl solution and pure aqueous solution to ionic strength [24]. Other electrochemical measurements have resulted in values for the absolute SHE potential of +4.7 V [15,17], which were obtained by measuring the potential difference between immersed vs. emersed electrodes. Reorientation of solvent on the electrodes upon emersion may account for the higher potential for the SHE than that obtained using other methods [35].

More recently, sequential hydration-free energies for a large series of positively and negatively charged ions (for up to 6 water molecules), in combination with a clever manipulation of thermodynamic cycles, have been used to obtain a value for $\Delta G_{\text{aq}}(\text{H}^+)$ [7,25,26,30]. These methods have the advantage that a model is not needed to obtain these values. Tissandier et al. introduced the cluster pair approximation [25], which improved on other related cluster-based methods [36,37], to obtain a value of -264.0 kcal/mol for $\Delta G_{\text{aq}}(\text{H}^+)$, which is essentially the same value obtained using the related cluster pair correlation method by Tuttle et al. [26], in which data for neutral water clusters are not required. Kelly et al. also obtained essentially the same value using a much larger data set and the cluster pair correlation method [7]. More recently, we evaluated this method with an even larger ion data set that includes 19 more ions, corresponding to 1129 additional experimental data points [30], than that used by Kelly et al. [7]. Using the expanded data set and this approach [30], a value of -259.3 kcal/mol was obtained for $\Delta G_{\text{aq}}(\text{H}^+)$, which is significantly less negative than the values obtained from the smaller sets of data. The dependence on the data set size suggests the uncertainty of these methods is larger than previously appreciated. In addition, an improved cluster pair correlation method was developed, which resulted in a value of -265.0 kcal/mol for $\Delta G_{\text{aq}}(\text{H}^+)$ using the same expanded data set [30]. Data for ions with extreme pK_{a} values are unreliable when used to obtain $\Delta G_{\text{aq}}(\text{H}^+)$ with the cluster pair correlation method, and these data were removed from the expanded data set [30]. There was only a subtle dependence of the value of $\Delta G_{\text{aq}}(\text{H}^+)$ on cluster size, and within the limits of the approximation used in the method, the “best” value obtained for $\Delta G_{\text{aq}}(\text{H}^+)$ using the expanded data set and improved cluster pair correlation method was -263.4 kcal/mol [30], which corresponds to the value for $E_{\text{abs}}(\text{SHE})$ of $+4.26$ V, which may not fully include the surface potential of water because of the small cluster sizes used. Although the precision of the cluster pair correlation method is excellent, the absolute uncertainty is challenging to confidently determine because (1) the entropy value obtained for the proton hydration free energy is anomalously high, (2) the proton hydration-free enthalpy values depend on cluster size, and to a much lesser extent, so do the Gibbs free energy values, and (3) the values obtained depend on the ion data set used and on the ion identity [30]. These results suggest that values obtained for $\Delta G_{\text{aq}}(\text{H}^+)$ may not have converged for clusters with only six water molecules [30]. However, including more data as it becomes available for larger clusters and more ions would provide a better indication of the overall accuracy of this approach.

As a result of the wide range of reported values for the absolute SHE potential from a number of different approaches, it is interesting to develop alternative and more direct approaches to obtain this value. We have recently developed three new gas-phase ion nanocalorimetry-based methods for obtaining absolute solution-phase reduction potentials [27–29]. In ion nanocalorimetry experiments [27–29,38–45], the absolute recombination energies of nanometer-sized hydrated metal ions that capture an electron are obtained from the number of water molecules lost from the reduced precursor clusters and directly related to absolute ion reduction potentials in aqueous solution. From three largely independent methods [27–29], values for the absolute SHE potential of $+4.05$, $+4.11$, and $+4.21$ V were obtained that are within 5 % of each other. For cases in which recombination between the captured electron and the hydrated ion does not result in direct metal ion reduction in the nanodrop, and a solvent-separated ion-electron pair is formed, the recombination enthalpies can be used to investigate electron hydration as a function of a discrete number of water molecules [39,40]. By extrapolating the recombination enthalpies for $\text{La}(\text{H}_2\text{O})_n^{3+}$ to infinite cluster size, a value for the absolute hydration enthalpy of the electron (-1.3 eV) was obtained [39], which is well within the wide range of values (-1.0 to -1.8 eV) that can be obtained from pulse radiolysis studies [46–49] and reported values for the absolute proton hydration enthalpy. The ion nanocalorimetry method is currently being calibrated using UV photodissociation experiments [50], which should improve the accuracy of these methods by eliminating the need for any theoretical models to obtain recombination energies. An advantage of one of our three methods for obtaining absolute solution-phase reduction potentials is that absolute potentials can be measured without any models, including a solvation model that is required by two of our other methods, making it the most direct approach to establish an absolute electrochemical scale entirely from

experimental data [27]. Here, we review these recent advances in performing gas-phase electrochemistry using hydrated ion nanocalorimetry.

HYDRATED ION NANOCALORIMETRY MEASUREMENTS

In ion nanocalorimetry experiments, which are related to the thermometer ion approach of Cooks and co-workers [51], a hydrated ion, $M^z(H_2O)_n$, where z is the formal charge of M , is isolated and reduced by capture of a thermal electron [27–29,38–45], or activated by other methods [50,52–55]. The recombination of the ion and the electron results in the deposition of energy into the cluster (corresponding to recombination energy, RE), cluster heating, and evaporation of water molecules from the reduced precursor, which results in the cooling of the cluster back to the initial starting temperature. For example, electron capture (EC) by $Cu(H_2O)_{29}^{2+}$ results in the loss of 16 or 17 water molecules from the reduced precursor, indicating that although the energy deposited into the cluster is large, the distribution of the deposited energy is exceedingly narrow [40]. Because the clusters, prior to EC, are isolated in ultrahigh vacuum and under the conditions of these experiments, radiative cooling is negligible [56], the energy removed by the lost water molecules is equal to the energy deposited into the precursor ion in accord with the Law of Conservation of Energy. Each water molecule removes the energy required for breaking the noncovalent interaction between the lost water molecule and the cluster (i.e., water molecule threshold binding energy, $E_{n,n-1}$), and, to a much lesser degree, the energy that statistically partitions into the translational, rotational, and vibrational modes of the products (E_{TRV}). The sum of the energy removed by the lost water molecules corresponds to the adiabatic ionization energy of the reduced cluster because the timescale of the experiments is much longer than the timescale required for water to reorganize about the reduced metal ion. That is, although capture of an electron may occur by a vertical process, there is sufficient time for the cluster geometry to reorganize prior to ion detection. Thus, any energy that is released as a result of solvent reorganization about the reduced ion results in additional heating of the cluster and contributes to the number of water molecules lost from the cluster. These physical measurements can be considered to be the inverse of determining threshold ionization energy values of molecules or ions using photoelectron spectroscopic methods (adding an electron vs. removing an electron), with the exception that the removal of an electron from a molecule or ion by a high-energy photon is generally a non-adiabatic process in agreement with the Frank–Condon principle.

For the ion nanocalorimetry measurements reviewed here, experiments were performed using a 2.75 T Fourier transform ion cyclotron resonance (FT-ICR) mass spectrometer with an external nano-electrospray ionization (nESI) source [57] and a temperature-controlled ion cell [58]. Briefly, gaseous hydrated ions were formed using nESI from aqueous solutions containing ~1–10 mM of salts of the metal ions of interest. The hydrated ions are transferred through 5 stages of differential pumping and trapped in the FT-ICR cell, which is surrounded by a copper jacket that is cooled to a temperature of 133 K. Ions are accumulated for 3–9 s, during which time dry nitrogen gas is introduced into the vacuum chamber surrounding the ion cell at a pressure of $\sim 10^{-6}$ Torr. After ion accumulation, a mechanical shutter is closed to prevent additional ions from entering the ion cell. A delay of 4–10 s after accumulation and before ion isolation ensures the ions have steady-state internal energy distributions close to the temperature of the Cu jacket and that the pressure returns to $\ll 10^{-8}$ Torr. More detailed descriptions of the experimental set-up have been presented elsewhere [42,45].

For EC experiments [27–29,38–45], a cluster ion of a single size is isolated from a broad distribution of hydrated ions by using the stored waveform inverse FT [59] technique to generate an excitation waveform that resonantly ejects undesired ions from the FT-ICR cell. Following a 40–50 ms delay, electrons are introduced into the ion cell from a heated dispenser cathode, which is located 20 cm from the cell center, by applying –1.4 or –1.5 V to the cathode for 40–120 ms. A delay of between 40 ms to 1.5 s between the end of electron irradiation and detection is used to ensure that dissociation of the reduced precursor ion is complete. Experiments performed on this instrument indicate that the energy

deposited upon EC does not depend on the cathode voltage or the trapping potentials of the FT-ICR cell over a very wide range of experimental conditions [45]. The cross-sections for ion-electron recombination, as measured in ion storage rings, increases rapidly as the relative kinetic energy between the ion and electron approaches zero [60–64]. In our experiments, although there is a wide spread of electron kinetic energies, it is the electrons for which the relative kinetic energy between the ion and electron is essentially zero that should be captured most efficiently [45].

For UV photodissociation experiments [50,52], individual cluster ions ($n < 90$), or an ensemble of three neighboring cluster ions are isolated ($n > 90$). The improved S/N obtained using the ensemble method makes it possible to acquire data for larger cluster ions in less time than for isolating cluster ions of a single size [65]. After isolation, ions are irradiated for between 0.5 and 5 s, prior to the simultaneous detection of precursor and product ions. For both EC and UV photodissociation experiments, the average number of water molecules lost due to either capture of an electron or absorption of a UV photon is corrected for dissociation resulting from the absorption of blackbody photons.

Effects of metal ion identity and hydration extent on the number of water molecules lost and electron capture reactivity

Metal ion identity

The amount of energy that is deposited into a hydrated ion upon EC depends on both the identity of the metal and on the extent of ion hydration. In Fig. 1, five product ion mass spectra are shown that result from the capture of an electron by a cluster containing 55 water molecules and $M(\text{NH}_3)_6^{3+}$, for $M = \text{Ru}$, Co , Os , Cr , and Ir [28].

Each of these cluster ions loses a different number of water molecules upon EC. For $M = \text{Ru}$, an average of 18.2 water molecules is lost, whereas for $M = \text{Ir}$, an average of only 14.2 water molecules is lost, indicating that the recombination energies of the clusters depend strongly on the identity of the ion in the nanodrop. Even though many water molecules are lost, the widths of the product ion distributions are very narrow (only 2 or 3 product ions wide) and the width and the shape of these distributions can be accurately accounted for by the distribution of energy that partitions into translations and rotations of the products for all the lost water molecules [38]. These results are consistent with each cluster having a singular value for the RE [38]. Interestingly, the number of water molecules lost is not correlated with the corresponding ionization energies of the bare metals [28]. For example, an average of 16.4 water molecules is lost for $M = \text{Cr}$, whereas 18.2 water molecules are lost for $M = \text{Ru}$, even though Ru has a third ionization energy (28.47 eV [66]) that is nearly 2.5 eV less than that of Cr (30.96 eV [66]).

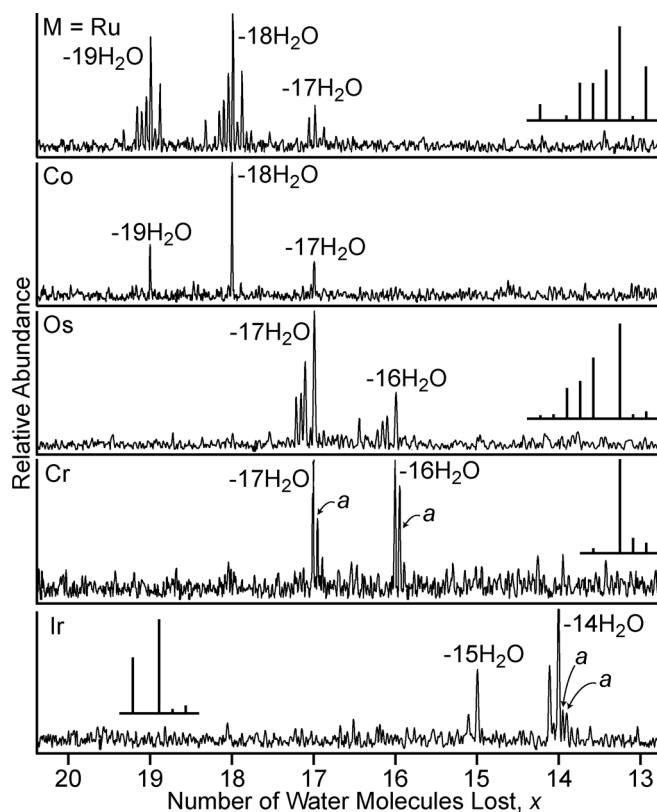


Fig. 1 Product ion mass spectra resulting from the capture of a thermal electron by isolated $M(\text{NH}_3)_6(\text{H}_2\text{O})_{55}^{3+}$, in which $M(\text{NH}_3)_6(\text{H}_2\text{O})_{55-x}^{2+}$ and $x\text{H}_2\text{O}$ are formed. The spectra are aligned on the x -axis by the number of water molecules lost. Theoretical isotope distributions for the most abundant product ions are shown in the insets. Ions that correspond to the loss of one or two ammonia molecules in addition to the water molecule loss are labeled by a . Figure adapted from [28].

Cluster size

The number of water molecules lost upon EC by $M^{z+}(\text{H}_2\text{O})_n$ also depends upon the size of the clusters. For example, the average number of water molecules lost upon capture of an electron by $M^{3+}(\text{H}_2\text{O})_n$, $M = \text{La}$ and Eu , for n up to 160, is plotted as a function of precursor cluster size in Fig. 2 [27,39]. At smaller cluster sizes, fewer water molecules are lost because the energy removed by each of the lost water molecules increases with decreasing size, that is, both the sequential binding energies and the amount of energy partitioning into the products increases as the cluster size decreases. At larger sizes, where the sequential water molecule binding energies and energy partitioning effects depend less strongly on cluster size, fewer water molecules are lost with increasing size because of the greater ion stability resulting from more effective ion solvation.

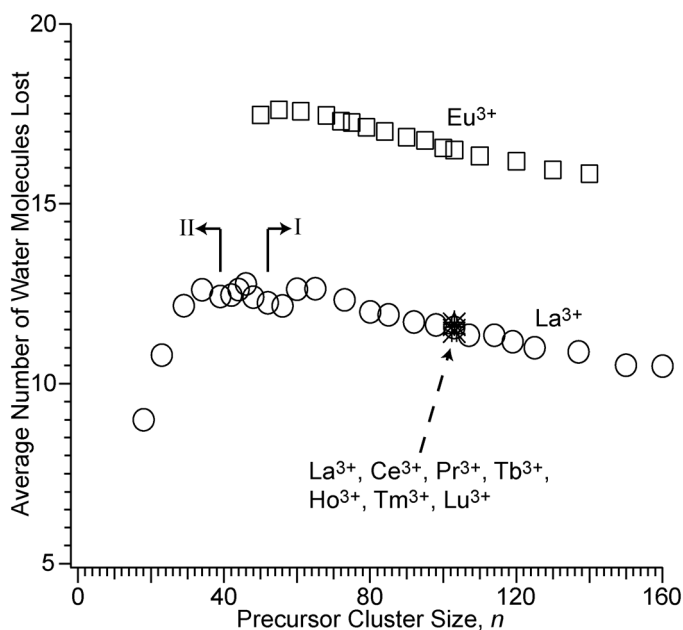
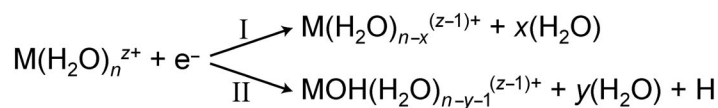


Fig. 2 Average number of water molecules lost as a result of EC by $M(\text{H}_2\text{O})_n^{3+}$ vs. n . Ion identity, M , is identified in figure. Solid arrows indicate cluster sizes for which either pathway I or II is exclusively observed for $M = \text{La}$. Figure adapted from [39].

Reactivity

In addition to the reduced cluster dissociating exclusively by the loss of water molecules (Scheme 1, pathway I), hydrated metal ions, such as $\text{Ca}^{2+}(\text{H}_2\text{O})_n$ [42] and $\text{La}^{3+}(\text{H}_2\text{O})_n$ [39], can also dissociate by the loss of a H-atom and water molecules upon EC, to form a metal hydroxide cluster (Scheme 1, pathway II). The branching ratio between these two dissociation pathways depends on the size of the precursor cluster and on the metal ion charge state and identity. For example, EC by $\text{La}^{3+}(\text{H}_2\text{O})_n$ results in exclusively pathway II dissociation for $n \leq 39$, whereas pathway I occurs for $n \geq 52$ [39].



Scheme 1 ECD pathways for $\text{M}^{z+}(\text{H}_2\text{O})_n$.

By contrast, EC by $\text{Ca}^{2+}(\text{H}_2\text{O})_n$ results exclusively in pathway II dissociation for $n \leq 22$, and pathway I occurs for $n \geq 30$ [42]. The transition from pathway II to I occurs over a wider range of cluster sizes at significantly larger sizes for La^{3+} ($n = 39\text{--}52$) than Ca^{2+} ($n = 22\text{--}30$). Furthermore, for EC by $\text{M}^{2+}(\text{H}_2\text{O})_{24}$ ($M = \text{Mg}, \text{Ca}, \text{Sr}, \text{and Ba}$), pathway II dissociation only occurs for $M = \text{Mg}$ but only pathway I occurs for $M = \text{Ba}$ [29]. For $M = \text{Ca}$, the ratio of product ions formed via pathway II to I is $\sim 2:1$, whereas that for Sr is $\sim 1:2$ [29]. These results all suggest that loss of a H-atom upon EC by hydrated metal ions is favored for ions with higher charge densities and for smaller cluster sizes. About two solvation shells or more are required to stabilize the reduced Ca^{2+} containing nanodrops against H-atom elimination upon EC, whereas for the La^{3+} containing nanodrops, nearly three complete hydration shells are required.

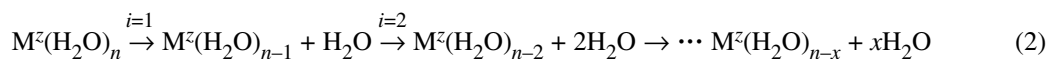
The number of water molecules lost via each dissociation pathway can also be different. For example, EC by $\text{Cu}(\text{H}_2\text{O})_{24}^{2+}$ results in the loss of an average of 16.3 water molecules via pathway I, but only 10.6 via pathway II [29]. In contrast, capture of an electron by $\text{Ca}^{2+}(\text{H}_2\text{O})_{24}$ results in essentially the same number of water molecules being lost via both pathways. These results indicate that the H-atom affinity of $\text{CuOH}^+(\text{H}_2\text{O})_{24}$ is relatively large in comparison to the hydrated CaOH^+ clusters of the same size. From the difference in the average number of water molecules lost via each pathway, the H-atom affinities of the corresponding hydroxide cluster can be obtained [29].

It is interesting to consider how EC results in the splitting of a water molecule to lose an H-atom from the smaller hydrated metal ions. Three possible mechanisms for the loss of a H-atom have been proposed [40]. In one mechanism, an ion pair between M^{z+}OH^- and H_3O^+ can be formed, either transiently or induced by the approach of the electron in a high- n Rydberg state, and a proton is shuttled to near the surface of the cluster in a Grotthuss-like mechanism. EC by the hydronium ion of $[\text{M}^{z+}\text{OH}^-(\text{H}_2\text{O})_{n-2}(\text{H}_3\text{O}^+)]^{z+}$ could result in reduction of the hydronium ion to form a H_3O radical. This radical is marginally stable in isolation [67], and upon formation via EC, may dissociate via H-atom loss, although this radical is stable on the microsecond timescale when hydrated [68]. Interestingly, the H_3O radical has been suggested as a possible form taken by the “hydrated electron” in bulk solution [69], although the cavity model for the hydrated electron, in which the excess electron is trapped in a cavity surrounded by water molecules, is more widely accepted [3]. Alternatively, the H-atom loss could result from direct electron attachment to an outer shell water molecule, resulting in the formation of H_2O^- , which dissociates via H-atom loss when formed in isolation [70]. This direct electron attachment to H_2O mechanism is supported by electronic structure calculations [71]. A third possible mechanism involves the direct reduction of the metal ion followed by an inter-cluster reaction, which results in formation of a hydrated metal hydroxide ion and ejection of a H-atom.

Obtaining ion-electron recombination energies

Recombination energies can be obtained either entirely from experimental data by calibrating the energy deposition using laser-generated photons of known energy (i.e., by directly relating the average number of water molecules lost from the cluster upon deposition of a known amount of energy) [50] or by modeling the energy removed by the lost water molecules [38]. The laser-photodissociation calibration approach to obtaining recombination energies has the advantage that these values can be obtained with high accuracy because no modeling of these data is necessary. The modeling approach to obtain RE values has the advantages that the extent of energy deposition can be rapidly obtained with reasonable accuracy and can be used to obtain the extent of internal energy deposition for cases in which electronic ion excitation results in incomplete conversion of the photon energy into the internal modes of the cluster. For example, we recently used ion nanocalorimetry to indirectly detect the laser-induced fluorescence of a hydrated ion (protonated proflavine) in the gas phase with high sensitivity [52]. In the future, such methods may be used to investigate the effects of a discrete number of water molecules on (1) the EC-induced chemi-luminescence of an ion that emits a photon upon one-electron reduction or (2) the dynamical motions of biomolecules tagged with Förster resonance energy-transfer dye pairs.

Upon rapid energy deposition into an ionic water cluster, such as for EC, the energy deposited into the precursor ion can be obtained from the average number of water molecules lost from the cluster and the sum of the $E_{n,n-1}$ and E_{TRV} values for all the lost water molecules [28,38,50]. Consider the sequential evaporation of x water molecules from a precursor cluster with n water molecules and an ion M^z , where z is the ion charge.



For the instantaneous conversion of electronic-to-vibrational energy, the energy value, E_D , required to “boil” off x number of water molecules, can be obtained from the following system of equations (eqs. 3–5, for each water molecule lost) [28,38,50].

$$U_0(T^*_0) = U_P(133\text{K}) + E_D \quad (3)$$

$$U_i(T^*_i) = U_{i-1}(T^*_{i-1}) - E_{n,n-1} - (5/2)kT^*_{i-1} \quad (4)$$

$U_i(T^*_i)$ is the average internal energy of the i th cluster, where i identifies the cluster by the number of water molecules evaporated to form this cluster and T^* is the effective temperature of the cluster. That is, $U_0(T^*_0)$ is the average internal energy of the activated precursor prior to losing any water molecules, which has an effective temperature of T^*_0 . $U_P(133\text{K})$ is the average internal energy of the precursor cluster, which is thermalized to ~ 133 K. The E_{TRV} values are given by $(5/2)kT^*_{i-1}$, which is obtained from Klots’ cluster evaporation model [72], where T^*_{i-1} is the effective temperature of the $i-1$ cluster and k is the Boltzmann constant. Average internal cluster energies are obtained from calculated harmonic frequencies for a smaller water cluster that are scaled by the number of vibrational degrees of freedom of the cluster of interest. The value of x is obtained from the ion nanocalorimetry experiments. For larger water clusters, there is only very limited data for measured $E_{n,n-1}$ values, so these values are obtained from the Thomson liquid drop model (TLDM) [73,74], which is an electrostatic model that can be used to calculate the sequential water molecule binding enthalpies to ionic water clusters using bulk physical properties. E_D is given by

$$E_D = \sum E_{n,n-1} + \left(\frac{5}{2}\right) k \sum T^*_{i-1} \quad (5)$$

where the first term on the right-hand-side of eq. 5 is the sum of the threshold binding energies and the second term is the sum of the E_{TRV} values for each water molecule lost from the precursor cluster. The system of equations given by eqs. 3–5 has the same number of unknowns (T^* values and E_D) as equations and can be solved to obtain values for E_D and T^* .

Cluster effective temperatures

As an example, the calculated effective temperatures for each sequential cluster formed upon EC by $\text{Cu}(\text{H}_2\text{O})_{32}^{2+}$ and $\text{Os}(\text{NH}_3)_6(\text{H}_2\text{O})_{55}^{3+}$ as a function of the number of molecules lost is shown in Fig. 3 [28]. Although the energy deposited into the internal modes of these clusters is about the same (~ 7.8 eV), $\text{Cu}(\text{H}_2\text{O})_{32}^{2+}$ is heated from an initial starting temperature of ~ 133 K to a calculated effective temperature of ~ 700 K, and $\text{Os}(\text{NH}_3)_6(\text{H}_2\text{O})_{55}^{3+}$ is only heated to an effective temperature of ~ 450 K [28]. Upon sequential water molecule loss from the reduced clusters, the effective temperatures of the reduced clusters return back to the initial starting temperature of the precursor cluster. The large difference in the effective temperatures of the respective reduced clusters is primarily a result of the osmium-containing cluster having nearly twice the number of vibrational degrees of freedom as the copper-containing cluster. The effective temperature also depends on the extent of internal energy deposition. For example, capture of an electron by $\text{Ru}(\text{NH}_3)_6(\text{H}_2\text{O})_{55}^{3+}$ (RE = 8.5 eV) results in an initial effective temperature of ~ 480 K, whereas that for $\text{Ir}(\text{NH}_3)_6(\text{H}_2\text{O})_{55}^{3+}$ (RE = 6.6 eV) is ~ 410 K [28]. In addition, the widths of the product ion distributions can be entirely accounted for by the distribution of energy removed by the water molecules lost [38].

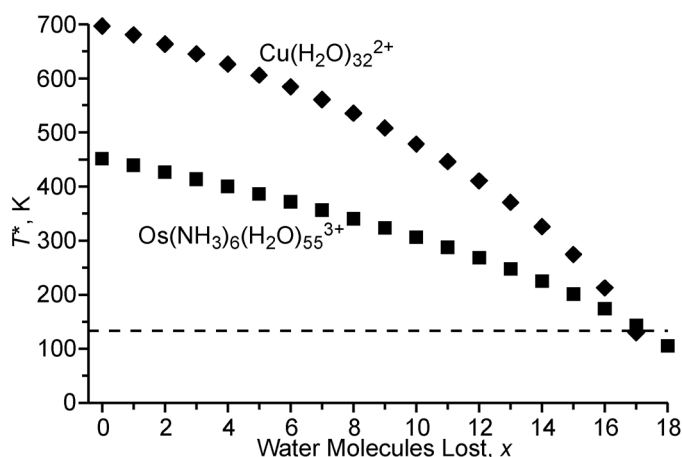


Fig. 3 Calculated effective temperatures (T^*) for the sequential cluster ions as a function of the number of water molecules lost from the reduced clusters, $\text{Cu}(\text{H}_2\text{O})_{32-x}^{2+}$ and $\text{Os}(\text{NH}_3)_6(\text{H}_2\text{O})_{55-x}^{3+}$. Figure adapted from [28].

Toward obtaining RE values entirely from experimental data

In order to calibrate the RE values obtained in EC experiments and to assess the models used to obtain these values, we have performed initial UV photodissociation experiments on hydrated metal ions [50]. The average number of water molecules lost from $\text{M}^{2+}(\text{H}_2\text{O})_n$ ($\text{M} = \text{Co}, \text{Fe}, \text{Mn}, \text{and Cu}$) upon absorption of either a 193-nm (6.4 eV) or 248-nm (5.0 eV) photon was measured for clusters with up to 124 water molecules (Fig. 4a) [50]. For a fixed photon energy, the average number of water molecules generally increases with increasing cluster size. For 248 nm, the average number of water molecules lost increases from a value of 8.6 water molecules to a value of 10.7 for an average precursor cluster size of 124. For 193 nm, a similar general trend is observed, but more water molecules are lost because the absorbed photon is 1.4 eV higher in energy than a 248-nm photon. For example, for a precursor cluster size of 30, an average of 11.0 water molecules are lost, and for a precursor cluster size of 130, an average of nearly 14 water molecules are lost. The average energy removed by each lost water molecule is close to the binding energies of water molecules to larger hydrated ions (~ 0.4 eV) [50,73], indicating that absorption of the UV photon results in full internal conversion, and that ion fluorescence or formation of a long-lived electronic excited state does not occur [52].

Fewer water molecules are lost from small clusters because, with decreasing cluster size, the water molecule binding energies increase and the clusters are heated to higher effective temperatures resulting in higher E_{TRV} values [50]. At the larger cluster sizes, the binding enthalpies and E_{TRV} values depend less strongly on cluster size and therefore the average water molecules lost also depend less strongly on cluster size. For clusters with more than ~ 40 water molecules, the average number of water molecules lost is insensitive to the identity of the divalent metals that have been investigated.

To evaluate the accuracy of the models for obtaining RE values (TLDM and E_{TRV} models), the energy deposited into the clusters was calculated using these models and compared to the known energy that is deposited into the internal modes of the clusters, i.e., the energy of the absorbed photon (Fig. 4b) [50]. In general, the calculated energy deposition values are nearly constant over a wide range in cluster sizes from ~ 40 to 130 water molecules. These values are on average 0.41 ± 0.13 and 0.38 ± 0.05 eV lower than the energy of the absorbed photons, which are 6.4 and 5.0 eV, respectively. Thus, the values obtained from the models underestimate the actual energy deposited into the clusters by an average of 6.5 and 7.7 % for the respective 6.4 and 5.0 eV absorbed photon. Because E_{TRV} values depend on both the photon energy and cluster size, and because the calculated energy deposited into the clusters does not depend significantly on cluster size for $n > \sim 40$, these results indicate that the dominant source of

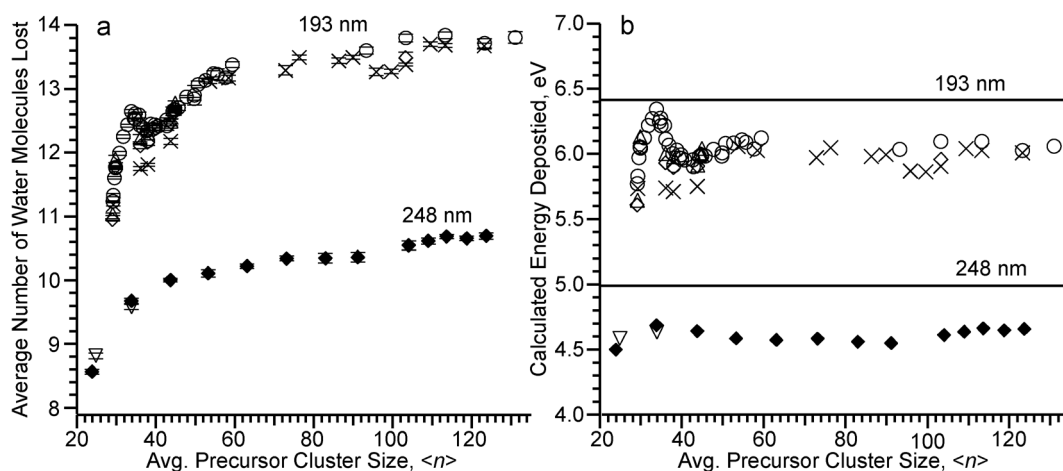


Fig. 4 (a) Average number of water molecules lost, and (b) calculated energy deposited into the clusters obtained using the measured average number of water molecules lost, the TLDM and the E_{TRV} model, for absorption of a 193-nm (6.4 eV) photon by $M(\text{H}_2\text{O})_n^{2+}$, $M = \text{Co}$ (\circ), Mn (\triangle), Fe (\diamond), and Cu (\times), and absorption of a 248-nm (5.0 eV) photon by $M(\text{H}_2\text{O})_n^{2+}$, $M = \text{Fe}$ (\blacklozenge) and CeNO_3 (∇) as a function of the average ensemble precursor cluster size. UV irradiation times vary from 0.5 to 5 s. Error bars indicate the propagated uncertainty from the noise in each mass spectrum. Figure adapted from [50].

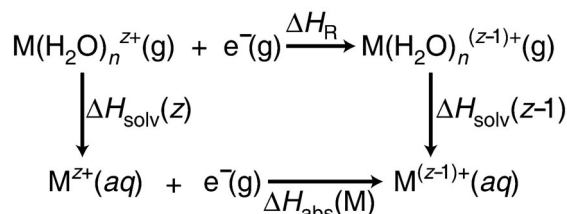
error in the calculated values is a result of the TLDM as opposed to the E_{TRV} model. As we have only recently begun to calibrate the RE values using this method and have only obtained data for hydrated divalent metal ions, and because the models provide reasonable accuracy for the purposes of discussing connecting gas-phase measurements to bulk thermochemistry, we will only report RE values that are obtained with the TLDM and E_{TRV} models here. Future work will expand the calibration data to a much wider range of photon energies, ion charge states, and larger cluster sizes.

CONNECTING GASEOUS HYDRATED IONS TO SOLUTION

We have introduced three largely independent methods for obtaining absolute solution-phase reduction potentials from gas-phase ion nanocalorimetry data [27–29], which are discussed in detail here. The common approach for all methods is that thermodynamic data for large clusters is connected to solution-phase data using thermodynamic cycles and condensed-phase data to obtain a value for the absolute SHE potential and hydration energy of the proton.

Single-cluster direct reduction method

In the “single-cluster direct reduction method” for obtaining a value for the absolute potential of the SHE, absolute solution-phase reduction potentials are obtained from the RE values of a single size-selected cluster containing an individual redox active ion that undergoes direct metal ion reduction [28]. These measurements, for clusters with either 55 or 32 water molecules attached, and the Scheme 2 thermodynamic cycle along with known solution-phase data were used to obtain a value for the absolute SHE potential.



Scheme 2 Thermodynamic cycle connecting gaseous hydrated ion measurements to solution.

For Scheme 2, the absolute recombination enthalpy of the precursor cluster (ΔH_{R} , which is readily obtained from the RE value) is connected to the absolute solution-phase reduction enthalpy of the redox active ion (ΔH_{abs}) by the absolute solvation enthalpies of the precursor cluster, $\Delta H_{\text{solv}}(z)$, and reduced cluster, $\Delta H_{\text{solv}}(z-1)$. From the Scheme 2 thermodynamic cycle,

$$\Delta H_{\text{R}} = \Delta H_{\text{abs}}(\text{M}) + \Delta \Delta H_{\text{solv}} \quad (6)$$

where $\Delta \Delta H_{\text{solv}}$ is the difference between the solvation enthalpies of the $z+$ and $(z-1)+$ cluster ions.

Because absolute ion solvation enthalpies of large ionic clusters cannot be directly measured, these values were calculated using the Born solvation model [75]. For the larger clusters, the ions are significantly solvated such that specific ion–solvent interactions are largely accounted for in the measured recombination enthalpy and thus, a continuum solvation model should account for the vast majority of the solvation enthalpy values for the ionic clusters. The absolute reduction Gibbs free energy of $\text{M}^{z+}(\text{aq})$ is obtained by combining the $\Delta H_{\text{abs}}(\text{M})$ value from our nanocalorimetry method with the absolute entropy term ($T\Delta S$) from solution-phase measurements. The absolute potential of each redox active species in solution is obtained using the Faraday equation.

In Fig. 5, the absolute solution phase Gibbs free energy values for one-electron reduction of the ions that are obtained from the cluster measurements [27,28] are plotted as a function of the corresponding relative Gibbs free energy values, $\Delta G_{\text{rel}}(\text{M})$, from the literature [76–81] that were obtained using traditional electrochemical methods (SHE = 0 V). This figure has been updated to include data for $\text{Eu}^{3+}(\text{H}_2\text{O})_n$, $n = 55\text{--}140$ [27]. A linear regression analysis results in a best fit line with a slope of 1.4, an intercept of -4.2 eV (or $+4.2$ V), and an R^2 value of 0.97, indicating that these values are directly correlated as expected by the Scheme 2 thermodynamic cycle. The y -intercept of this line corresponds to a value for the absolute SHE potential of $+4.2$ V, with a precision of ± 0.1 V. The average value obtained for the absolute SHE potential from the Eu data is -4.18 V with a standard deviation of ± 0.02 V, indicating that the method is remarkably precise over a wide range of cluster sizes.

The slope of the Fig. 5 line is higher than the expected value of 1, at least in part, because the deviation between the RE values obtained from the models and the actual values does depend slightly on the magnitude of the RE value. Use of the Born solvation model also introduces uncertainty, which may account partially for this deviation. In addition, there is also uncertainty in the measured solution-phase reduction potentials. For example, it is challenging to obtain accurate half-cell reduction potentials for reactions that do not have well-defined reverse oxidation waves, such as for $\text{M}(\text{NH}_3)_6^{3+/2+}$ ($\text{M} = \text{Co}, \text{Cr}, \text{and Ir}$). A more detailed analysis of the sources of uncertainty in obtaining these values is discussed elsewhere [28].

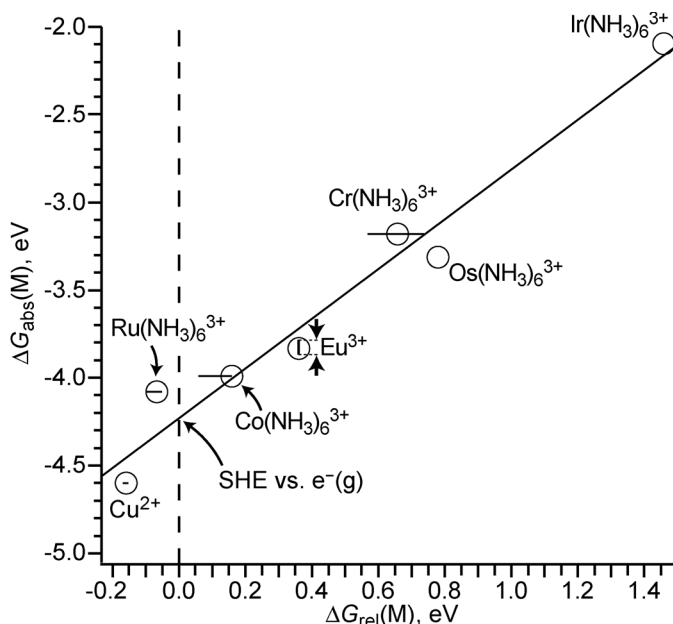
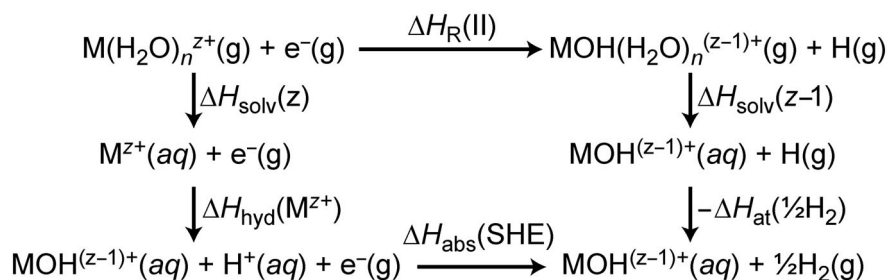


Fig. 5 Absolute solution-phase reduction free energies, $\Delta G_{\text{abs}}(\text{M})$, obtained from gas-phase reduction of $\text{Cu}(\text{H}_2\text{O})_{32}^{2+}$, $\text{Eu}(\text{H}_2\text{O})_{55}^{2+}$, and $\text{M}(\text{NH}_3)_6(\text{H}_2\text{O})_{55}^{3+}$, $\text{M} = \text{Ru}, \text{Co}, \text{Cr}, \text{Os}, \text{and Ir}$, as a function of the relative reduction free energies, $\Delta G_{\text{rel}}(\text{M})$, referenced to the SHE from solution measurements for the same redox couples. The y-axis (dashed line) intercept of the linear regression best fit line (solid line) corresponds to the absolute SHE potential. The vertical bar marked with black vertical arrows represents the range of absolute reduction energies obtained from single-cluster measurements for $\text{Eu}(\text{H}_2\text{O})_n^{3+}$, $n = 55$ to 140 (average $E_{\text{abs}}(\text{SHE})$ value of -4.18 V, with a standard deviation of 0.02 V, is obtained from the Eu data for $n = 55$ –140) [27]. Horizontal bars indicate a select range of reported solution-phase values. Figure updated from [28].

Single-cluster hydrolysis method

For comparably smaller hydrated ions, EC can result in a second dissociation pathway (Scheme 1, pathway II), in which a H-atom is lost in addition to water molecules, to form a solvated metal hydroxide ion, as opposed to exclusively losing water molecules from the reduced precursor ion (pathway I) [29]. The energy deposited into the precursor ion upon EC via pathway II can be related to the absolute SHE potential using the thermodynamic cycle shown in Scheme 3. For this thermodynamic cycle, the enthalpy of reducing the nanodrop and losing a H-atom, $\Delta H_{\text{R}}(\text{II})$, which is obtained from the number of water molecules lost to form pathway II ions upon EC by the precursor cluster, is directly related to the absolute reduction enthalpy of the SHE, $\Delta H_{\text{abs}}(\text{SHE})$, by the absolute solvation enthalpies of the respective precursor and product ion clusters, the solution-phase hydrolysis enthalpy of M^{2+} , $\Delta H_{\text{hyd}}(\text{M}^{2+})$, and the atomization enthalpy of $\frac{1}{2}\text{H}_2$, $\Delta H_{\text{at}}(\frac{1}{2}\text{H}_2)$.

For this method, we obtained $\Delta H_{\text{R}}(\text{II})$ values from the average number of water molecules lost from $\text{M}^{2+}(\text{H}_2\text{O})_{24}$ upon EC and dissociation via pathway II for nine different metal ions (Mn, Fe, Co, Ni, Cu, Zn, Mg, Ca, and Sr) which ranged from 110.1 to 115.3 kcal/mol for Sr to Cu, respectively. Values for the enthalpy of metal ion hydrolysis [82], for each metal ion, and the atomization enthalpy of H_2 [83] were obtained from the literature. $\Delta G_{\text{abs}}(\text{SHE})$ is obtained from $\Delta H_{\text{abs}}(\text{SHE})$ from the absolute entropy term as was done for the previous method. The average of the $\Delta G_{\text{abs}}(\text{SHE})$ values obtained from each of the 9 measurements results in a value of -4.05 eV, or $+4.05$ V, with a standard deviation of only ± 0.02 V (updated [27] from ref. [29]), which is in excellent agreement with the sin-



Scheme 3 Thermodynamic cycle connecting cluster measurements to ion hydrolysis and the SHE reaction in solution.

gle-cluster direct reduction method, especially when considering that these clusters are relatively small and should include just over two solvation shells surrounding the metal ions.

Because the $\Delta H_{\text{abs}}(\text{SHE})$ and $\Delta H_{\text{at}}(\frac{1}{2}\text{H}_2)$ are constants, and because the solvation enthalpies of the precursor and product clusters should not depend strongly on the identity of the divalent metal for these relatively large clusters, the $\Delta H_{\text{R}}(\text{II})$ values should be strongly correlated with the metal ion hydrolysis enthalpies (Scheme 3). In Fig. 6, $\Delta H_{\text{R}}(\text{II})$ values are plotted as a function of hydrolysis enthalpies. The best fit line to this data has a slope of 1.2 ± 0.1 and an R^2 value of 0.95, which is an excellent correlation considering the small range in enthalpy values (~ 5 kcal/mol) [29].

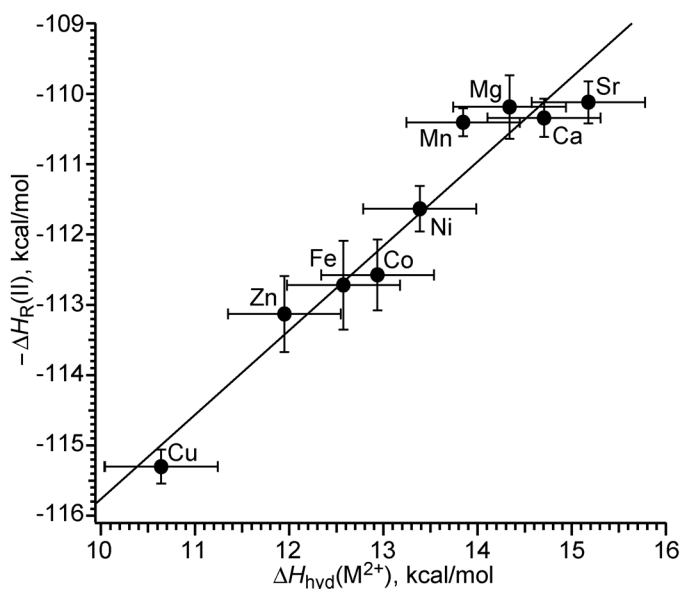


Fig. 6 Negative of $\Delta H_{\text{R}}(\text{II})$ values for $\text{M}(\text{H}_2\text{O})_{24}^{2+}$, $\text{M} = \text{Mg}, \text{Ca}, \text{Sr}, \text{Ba}, \text{Mn}, \text{Fe}, \text{Co}, \text{Ni}, \text{Cu}$, and Zn , obtained from ion nanocalorimetry data, vs. the enthalpy of solution-phase hydrolysis for M^{2+} obtained from the literature. Vertical black bars represent the uncertainty propagated from the signal-to-noise level and the horizontal error bars correspond to one standard deviation in the entropy correction. Figure updated from [29].

Extrapolation method: Toward measuring the absolute SHE potential without models

An alternative strategy, which does not require a solvation model for calculating absolute ion cluster solvation enthalpies, is to extrapolate recombination enthalpy values as a function of the geometric

dependence of the cluster reduction energy to infinite cluster size [27]. The solvation enthalpy of a cluster ion is proportional to the inverse of the cluster radius (R) for sufficiently large ionic clusters that can be approximated as spheres. Considering that the volume of a sphere is proportional to n , and that the radius is proportional to $n^{1/3}$, eq. 6 can be rearranged to eq. 7, where C is a constant and $\Delta H_R(n)$ is the recombination enthalpy of $M^z(\text{H}_2\text{O})_n$ that depends on n .

$$\Delta H_R(n) = \Delta H_{\text{abs}}(M) + Cn^{-1/3} \quad (7)$$

A plot of the measured reduction enthalpies as a function of $n^{-1/3}$ should result in a line with a y-axis intercept of $\Delta H_{\text{abs}}(M)$, for clusters that are large enough that they can be approximated as spheres. That is, the absolute reduction enthalpy can be obtained by extrapolating $\Delta H_R(n)$ values to infinite cluster size as a function of $n^{-1/3}$.

In Fig. 7, the $-\Delta H(n)$ values for $\text{Eu}^{3+}(\text{H}_2\text{O})_n$ ($n = 50\text{--}140$), obtained from ion nanocalorimetry, are shown vs. $n^{-1/3}$ [27]. These data are linear from $n = 55\text{--}140$, and the best fit line to this data has an intercept of 3.03 eV, a precision of ± 0.06 eV, and an R^2 value of 0.997. The linear dependence over this wide range of cluster sizes indicates that ion solvation accounts for the vast majority of the decrease in the recombination enthalpies with increasing cluster sizes for these clusters. The y-axis intercept corresponds to the absolute one-electron reduction enthalpy of Eu^{3+} in aqueous solution (-3.03 eV). Combining the absolute bulk one-electron reduction enthalpy value for $\text{Eu}^{3+}(\text{aq})$ with the absolute entropy obtained from experimental measurements, a value of $+3.75$ V for the absolute solution-phase reduction potential of Eu^{3+} is obtained [27]. From this absolute value and the measured relative reduction potential of $\text{Eu}^{3+/2+}(\text{aq})$ vs. the SHE (-0.36 V), a value of $+4.11$ V for the absolute SHE potential is obtained [27]. This value is in excellent agreement with the values obtained via both the single-cluster direct reduction ($+4.21$ V) and the hydrolysis ($+4.05$ V) methods (within 5 %).

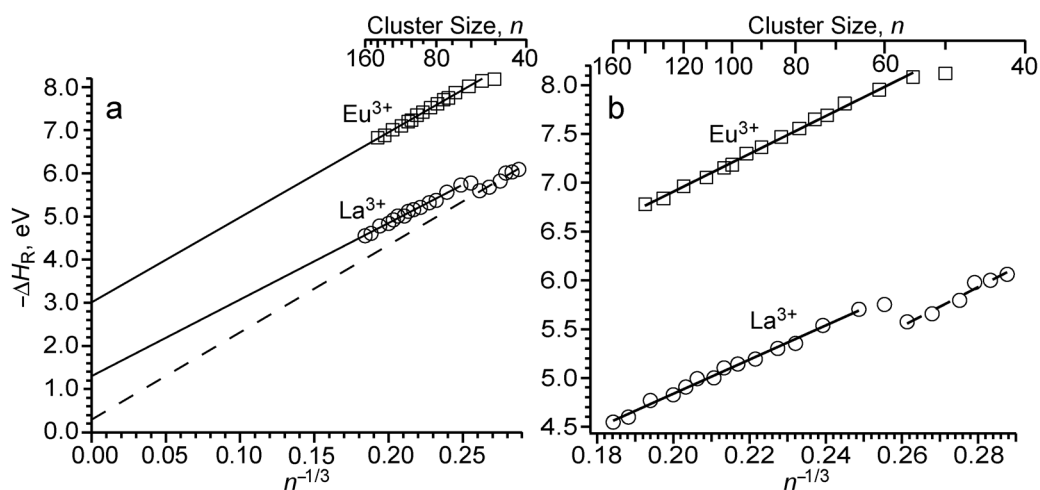


Fig. 7 (a) Negative recombination enthalpies of $M^{3+}(\text{H}_2\text{O})_n$ ($M = \text{Eu}$ and La) vs. $n^{-1/3}$, and (b) a magnified view of the left panel is shown. The precursor cluster sizes are indicated on the top horizontal axis. The intercept of the linear regression best-fit line to the Eu data corresponds to the absolute solution-phase reduction enthalpy of $\text{Eu}^{3+/2+}$ (-3.03 eV; standard deviation of 0.06 eV), and that for the La data corresponds to the absolute hydration enthalpy of the electron (-1.34 ; standard deviation of 0.09 eV). Figure adapted from [27,39].

Sources of uncertainty

Because the extrapolation method does not require a solvation model to calculate absolute cluster solvation enthalpies, this method is expected to be the most accurate of our three nanocalorimetry meth-

ods for obtaining the absolute SHE potential because uncertainty originating from using these models is eliminated. The precision of the method is also excellent (± 0.06 V), which reflects the reproducibility of these measurements over a wide range in cluster sizes. The greatest uncertainty in the value obtained for the absolute SHE potential is likely to be in the recombination enthalpies that were obtained from models that underestimate these values by $\sim 7\%$. This source of uncertainty can be eliminated by calibrating recombination enthalpy values using UV photodissociation data [50], such that a value for the absolute SHE potential can be obtained entirely from experimental data without modeling.

The accuracy of these methods should also be improved by extending these measurements to larger clusters. Many of the performance characteristics of the apparatus used to make these measurements, including trapping efficiency, improve quadratically with the strength of the magnetic field. At 7.0 T, significantly larger clusters could be investigated, which should increase both the accuracy and precision of our extrapolation method when combined with the laser calibration data.

Surface potential of water

Because an absolute potential can be defined as either including or excluding the surface potential of water, it is important to consider whether the nanocalorimetry experiments include a contribution from the surface potential of the nanodrops. Consider two concentric hollow spheres with radii of R_I and R_{II} that are oppositely charged ($-Q$ and $+Q$, respectively) and superimposed (Fig. 8). These two oppositely charged spheres are a simplified representation of an imbalance of the electric field that can occur due to the orientation of water molecules at the surface of the clusters. The electric field in the region between the two spheres ($R_I < R < R_{II}$) is given by eq. 8, where ϵ_0 is the vacuum permittivity.

$$E = -\frac{Q}{4\pi\epsilon_0 R} \quad (8)$$

The electric potential (Φ) of bringing a negative test charge from infinite distance (taken as 0 V) to the center of the two spheres is given by eq. 9.

$$\Phi = -\int_{\infty}^R E dR = -\frac{Q}{4\pi\epsilon_0} \left(\frac{1}{R_I} - \frac{1}{R_{II}} \right) \quad (9)$$

Although the electric field inside the inner sphere is zero, the electric potential referenced to an electron at infinite distance is non-zero in the case where there is a surface potential. Thus, our nanocalorimetry measurements include the effects of the surface potential of the nanodrop.

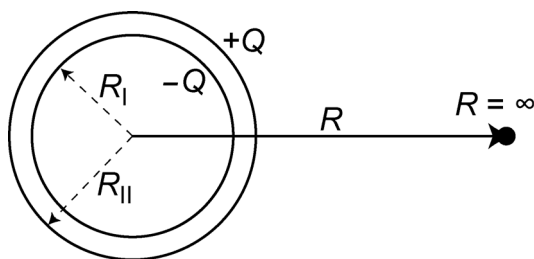


Fig. 8 Diagram of two hollow and superimposed concentric spheres that are oppositely charged ($-Q$ and $+Q$) with respective radii of R_I and R_{II} . The electric potential (Φ) at the center of the oppositely charged spheres ($R = 0$), referenced to infinite distance ($R = \infty$), is defined as the integral of the electric field with respect to R from $R = \infty$ to 0 and is non-zero for $R_I \neq R_{II}$ and $Q \neq 0$. This simple model illustrates the concept of a surface potential resulting from the orientation of solvent molecules at the surface of a spherical droplet, which can be non-zero, even though the electric field at $R = 0$ and ∞ is 0.

To compare values for the absolute SHE potential obtained from our cluster measurements to previously reported values that include the surface potential of water, it is important to consider the surface structure of the nanodrops vs. that for bulk liquid water. A powerful way to obtain information about the surfaces of gaseous hydrated ions is using infrared photodissociation (IRPD) spectroscopy experiments [84–92]. Free O–H stretching bands of water molecules at the surface of the nanodrops can be readily observed and assigned to water molecules that accept either one or two hydrogen bonds and donate either one or no hydrogen bonds to another water molecule. IRPD spectroscopy results for $M(\text{H}_2\text{O})_n^{2+}$ ($M = \text{Mg}, \text{Ca}, \text{and Ba}$), for n up to 69 [84–86], indicate that there are essentially no single acceptor water molecules at the cluster surface for clusters with ~ 30 or more water molecules, and these spectra essentially do not change at larger sizes. Ensemble IRPD results for $M(\text{H}_2\text{O})_{35-36}$ ($M = \text{I}^-, \text{Cl}^-, \text{HCO}_3^-, \text{OH}^-, \text{tetrabutyl-}, \text{tetrapropyl-}, \text{and tetra-methylammonium}, \text{Cs}^+, \text{Na}^+, \text{Li}^+, \text{H}^+, \text{Ba}^{2+}, \text{Ca}^{2+}, \text{Co}^{2+}, \text{Mg}^{2+}, \text{La}^{3+}, \text{and Tm}^{3+}$) [88] indicate that there are significantly more surface water molecules that accept two H-bonds and donate a single H-bond than other free O–H water molecules for these relatively large clusters that contain a wide array of different ions. The dominance of double H-bond accepting and single H-bond donating water molecules in these nanodrops is consistent with what is known about the surface structure of bulk liquid water [93–97]. The frequencies of the free O–H stretches of surface water molecules that accept two hydrogen bonds and donate one hydrogen bond depend predominantly on the charge state of the ion, and to a much less extent on the identity of the ion. The frequency of this band, extrapolated to zero net charge, is essentially the same as the free O–H stretch of water at the air–water interface obtained from sum frequency generation (SFG) experiments [88]. In addition, the fully bonded OH stretch region of these nanodrops is very similar to that measured for bulk liquid water. The sum total of these results indicates that for the larger nanodrops, the hydrogen bonding structure of water at the surface of the nanodrops is similar to that at the air–water interface of bulk liquid water, and that the water inside the droplet is more liquid-like as opposed to ice-like, which is consistent with the water molecule binding enthalpies of larger nanodrops that are closer to the bulk heat of liquid water vaporization than ice sublimation [50].

It is also important to consider structure of the local solvation shell surrounding the ion in the nanodrop. One property to characterize ion solvation is the ion coordination number (CN). Results from IRPD experiments for $\text{Ca}^{2+}(\text{H}_2\text{O})_n$ indicate that the ion CN in these clusters is 6, for n less than 12 [84], which is consistent with results from other experiments [98–101] and theory [100–102]. For clusters with 12 or more water molecules, IRPD experiments indicate that the CN of Ca^{2+} is 8, which is consistent with the results from many solution-phase studies and suggests the coordination environment for Ca^{2+} in the larger nanodrops is similar to that in bulk water [85]. The charge separation reactivity of hydrated trivalent metal ions, for a wide range of lanthanides (14 different ions), for which these clusters lose $\text{H}^+(\text{H}_2\text{O})_x$ to form $\text{MOH}^{2+}(\text{H}_2\text{O})_y$ at cluster sizes between 17 and 21 water molecules, is strongly correlated to the solution-phase hydrolysis data [87]. In addition, as described above, there are strong correlations between (1) the gas-phase reduction energies of nanodrops containing redox active ions and the one-electron reduction potentials of the fully solvated ions in bulk solution (Fig. 5) [28], and (2) the $\Delta H_{\text{R}}(\text{II})$ values for nine different divalent metals and the solution-phase hydrolysis enthalpies (Fig. 6) [29]. These results all suggest that the local environments of the metal ions in the nanodrops are similar to that in bulk solution.

The results from IRPD experiments suggest that both the structure at the surface of the nanodrops and the CN of the ions in the nanodrops resemble that for bulk liquid water. Although the value for the surface potential of water has not been directly measured and is not known accurately, many estimates indicate that this value is very small [103]. Also, the value obtained for $\Delta G_{\text{abs}}(\text{SHE})$ obtained from the extrapolation method for large nanodrops (up to $n = 140$) [27] is very close to the value obtained from the largely independent hydrolysis nanocalorimetry method that was obtained from data for smaller clusters ($n = 24$) containing divalent ions [29], indicating that any differences in surface potential for clusters in this size range do not measurably affect our results. These results all suggest that any differ-

ence between surface structure of the nanodrops and bulk solution is minor and should contribute negligibly to the uncertainty in the absolute reduction enthalpy measurements.

Real proton hydration free energies

The real hydration energy of the proton can be obtained from the absolute SHE potentials obtained from our ion nanocalorimetry methods using eq. 1. The values of +4.05, +4.11, and +4.21 V for the absolute SHE potential correspond to standard real proton hydration free energies of -269.1 , -267.7 , and -265.4 kcal/mol, respectively [27]. These values are more negative than the “best” value obtained for the standard absolute proton hydration energy from the improved cluster pair correlation method with an expanded data set (-263.4 kcal/mol) [30], and are close to that directly calculated by Goddard and co-workers (-265.4 kcal/mol) [31], although both of these latter values may not fully account for the surface potential of water because of the small cluster sizes used. The value for the real proton hydration energy obtained by Farrell and McTigue from experiment and a theoretical model (-260.0 kcal/mol) [24] is significantly higher than that obtained via the ion nanocalorimetry methods. However, because the RE values obtained using the TLDM and E_{TRV} models underestimate the energy deposition [50], calibration of the ion nanocalorimetry using UV photodissociation experiments should result in values that are less negative for the real proton hydration energy and would be closer to the value reported by Farrell and McTigue [24].

ELECTRON HYDRATION

Many hydrated ions do not have well-known one-electron reduction potentials owing to the rate for one-electron reduction being slower than that for a subsequent electron transfer or for the simultaneous transfer of multiple electrons to the ion. This highlights the challenge in controlling the precise number of electrons that are transferred to an ion using traditional electrochemical methods in solution. For hydrated metal ions that do not have well-known one-electron reduction potentials, such as for divalent Mg, Ca, Sr, and Ba, and nearly all of the trivalent lanthanides, it is interesting to consider what occurs upon capture of a single electron by a water cluster that contains these types of ions, given that in the gas phase, the number of electrons transferred to the ion can be carefully controlled.

Ion–electron pair formation in nanodrops.

In Fig. 2, the average number of water molecules lost upon capture of a single electron by $M^{3+}(\text{H}_2\text{O})_n$ ($M = \text{La}$ and Eu ; n up to 160) and $M^{3+}(\text{H}_2\text{O})_{103}$ ($M = \text{Ce}$, Pr , Tb , Ho , Tm , and Lu) is plotted vs. the precursor cluster size [27,39]. The extent of water loss depends on the cluster size. For $n = 103$, the Eu-containing cluster loses an average of 16.0 water molecules, which is much greater than that lost by $M^{3+}(\text{H}_2\text{O})_{103}$, for $M = \text{La}$, Ce , Pr , Tb , Ho , Tm , and Lu [27,39]. These latter lanthanide-containing clusters all lose nearly the same number of water molecules despite the differences in the third ionization energies of the bare metal atoms, which range from a value of 19.18 to 23.68 eV for La to Tm, respectively. Other clusters containing trivalent metal ions ($M(\text{NH}_3)_6(\text{H}_2\text{O})_{55}^{3+}$, $M = \text{Ru}$, Co , Os , Cr , Ir) lose both *different* numbers of water molecules (between 14 and 19) [28] than each other and *more* water molecules than $\text{La}(\text{H}_2\text{O})_{60}^{3+}$ (up to ~ 5.6 more for Ru than La). These results all indicate that upon capture of a single electron by $\text{La}^{3+}(\text{H}_2\text{O})_n$, which results in dissociation by exclusively water molecule loss (pathway I, $n \geq 42$), formation of a solvent-separated ion–electron pair occurs in the nanodrops, which also occurs for $M^{3+}(\text{H}_2\text{O})_{103}$, $M = \text{Ce}$, Pr , Tb , Ho , Tm , and Lu [39]. That is, a water cluster containing both M^{3+} and e^- are formed and these two oppositely charged ions do not recombine. Similarly, capture of a single electron by $M^{2+}(\text{H}_2\text{O})_{32}$, $M = \text{Mg}$, Ca , Sr , and Ba , results in nearly the same average number of water molecules lost (ca. 10.1), despite the second ionization energies of the unsolvated atoms ranging from 10.0 to 15.0 eV for Ba to Mg, respectively [40,41]. By contrast, $M^{2+}(\text{H}_2\text{O})_{32}$, $M = \text{Mn}$, Fe , Co , Ni , Cu , and Zn , all lose *more* water molecules (up to an average of 16.35 for $M = \text{Zn}$ and Cu , respectively) than for $M = \text{Mg}$, Ca , Sr , and Ba , and *different* numbers of water molecules (between 11.31 and 16.35 for Zn and Cu, respectively) than each other [38]. These results also indicate

that upon EC by water clusters containing divalent $M = \text{Mg, Ca, Sr, and Ba}$, a solvent-separated M^{2+} and electron pair is formed when water molecules are exclusively lost (pathway I, $n > 22$ for $M = \text{Ca}$) [40,41]. These gas-phase results are consistent with solution-phase redox results as the one-electron reduction potentials for M^{3+} ($M = \text{La, Ce, Pr, Tb, Ho, Tm, and Lu}$) and M^{2+} ($M = \text{Mg, Ca, Sr, and Ba}$) in solution have not been measured, whereas those for Eu^{3+} , $M(\text{NH}_3)_6^{3+}$ ($M = \text{Ru, Co, Cr, Os, Ir}$) and Cu^{2+} are readily measured. For these ions, the gas-phase nanodrop reactivity is correlated to the bulk redox chemistry.

It is interesting that the one-electron reduction potentials for the divalent transition metals M^{2+} ($\text{Mn, Fe, Co, Ni, and Zn}$) have not been reported, yet the metal ion is directly reduced upon EC by clusters containing either 24 or 32 water molecules and one of these transition-metal ions. These results indicate that for these ions, the directly reduced metal ions are more stable than the corresponding solvent-separated ion–electron pairs in nanodrops of these sizes. Future experiments will investigate these ions in more detail to better understand the competition between direct-metal ion reduction vs. ion–electron pair formation.

It is quite remarkable that metal ions in a 3+ charge state can be separated from an excess electron in these water clusters. To further investigate this phenomenon, 300 K OPLS-2005 molecular dynamics (MD) simulations were performed on model water clusters ($n = 10\text{--}160$) containing a triply charged metal ion and I^- that are initially in direct contact (contact ion pair) at a distance of 2.6 Å and situated in the center of the clusters [39]. I^- was used because it has an ionic radius that is about the same as the radius of the cavity, which has been suggested to trap the hydrated electron in ice, and it has been used as a model for the hydrated electron in other MD simulations [104]. Within about 200 ps, the contact ion pair separates to form a solvent-separated ion pair ($n > \sim 10$) in which the iodide tends to be at the surface of the clusters ($n < \sim 100$) or in a solvent shell near the surface of the cluster ($n > \sim 100$), and with the metal ion tending to be near the center of the clusters [39]. The equilibrium distance between the Mo^{3+} and I^- ions in the droplets increases with increasing cluster size. For example, the average equilibrium distance between the oppositely charged ions is just over 4 Å for $n = 20$ and steadily increases to a value of ~ 6.2 Å for $n = 160$. The inverse of the average equilibrium distances, which is proportional to the Coulomb energy between the ions, is generally linear as a function of $n^{-1/3}$. This result is consistent with other calculations, which indicates that vertical ionization energies for water clusters containing either a surface-bound or an internally solvated electron should be linear as a function of $n^{-1/3}$ [105].

Extrapolation of recombination enthalpies to bulk water

The recombination enthalpies of $\text{La}(\text{H}_2\text{O})_n^{3+}$ are plotted vs. $n^{-1/3}$ (Fig. 7) in order to connect these values to that for the corresponding electron hydration enthalpy in aqueous solution [39]. The recombination enthalpy values monotonically and linearly decrease with increasing cluster size for $n = 42\text{--}56$. However, the value for $n = 60$ is significantly larger than that for $n = 56$, and these values decrease monotonically and linearly for $n = 60\text{--}160$ with increasing cluster size. The break at $n \sim 58$ is attributed to a structural transition from a surface-solvated electron to a more fully solvated electron. In contrast, the recombination enthalpies for Eu^{3+} -containing clusters decrease linearly and monotonically for $n = 55\text{--}140$, indicating that the transition observed for La^{3+} -containing clusters is not a result of a cluster-size-dependent phase transition.

A linear regression best fit line to the La data for $n = 65\text{--}160$ results in an R^2 value of 0.993 and y-axis intercept of 1.34 (± 0.09 eV). The y-axis intercept corresponds to a value for the bulk hydration enthalpy of the electron of -1.34 eV. This value is well within a wide range of values (-1.0 to -1.8 eV) that can be obtained from various thermodynamic cycles, condensed phase data, and estimates for the hydration enthalpy of the proton. Our method has the advantage that it is completely independent of previous methods for obtaining the hydration enthalpy of the electron and does not require a value for the proton hydration enthalpy.

The best fit line for the La data for $n = 42\text{--}56$ results in an R^2 value of 0.962 and a y -axis intercept of $+0.3 \pm 0.5$ eV. To the extent that the excess electron is delocalized on the cluster surfaces of these smaller clusters, this latter value corresponds roughly to a value of ca. -0.3 eV for the conduction band of bulk water, i.e., the energy for forming a delocalized electron in bulk water from the gas phase with no kinetic energy. This value (-0.3 ± 0.5 eV), along with the value obtained using this nanocalorimetry method, but for $\text{Ca}(\text{H}_2\text{O})_n^{2+}$ ($+0.6$ eV) [40], brackets an estimate for this value of ~ 0 for both ice and liquid water [1,4].

CONCLUSIONS

We have introduced three largely independent methods that use ion nanocalorimetry measurements to obtain a value for the absolute SHE potential that ranges from $+4.05$ to $+4.21$ V. These values are lower than the actual absolute SHE potential because the models used to obtain RE values from the nanocalorimetry experiments underestimate the energy deposited into the clusters by $\sim 7\%$. Our nanocalorimetry extrapolation method is particularly promising because, when combined with the UV photodissociation calibration approach, it eliminates the need for any models, making this the most direct approach to establishing an absolute electrochemical scale entirely from experimental data. For cases in which EC results in formation of a solvent-separated ion–electron pair, the extrapolation approach can also be used to obtain a value for the absolute hydration enthalpy of the electron entirely from experimental data. From these nanocalorimetry methods, it is feasible that a value for the absolute SHE potential and real proton hydration energy can be obtained with comparable accuracy to that with which relative potentials and ion solvation energies can be measured in solution, which would provide routes to establishing accurate absolute electrochemical and ion solvation scales.

ACKNOWLEDGMENTS

We thank the National Science Foundation (Grant CHE-1012833) for generous financial support and the Eastman Chemical Co. for sponsoring an ACS Division of Analytical Chemistry Summer Fellowship for W.A.D. Acknowledgment is made to the donors of the Petroleum Research Fund, administered by the American Chemical Society (No. 47916-AC6), for support of this research. We also thank Dr. Ryan D. Leib, Jeremy T. O'Brien, Maria Demireva, Dr. Matthew F. Bush, Bogdan Negru, and Prof. Daniel M. Neumark for their contributions to some of the work reviewed here. We also thank Dr. Alan L. Rockwood and Profs. Peter B. Armentrout, John I. Brauman, and Jack Simons for helpful discussions.

REFERENCES

1. J. V. Coe. *Int. Rev. Phys. Chem.* **20**, 33 (2001).
2. G. A. Voth. *Acc. Chem. Res.* **39**, 143 (2006).
3. J. M. Herbert, L. D. Jacobson. *Int. Rev. Phys. Chem.* **30**, 1 (2011).
4. J. V. Coe, S. M. Williams, K. H. Bowen. *Int. Rev. Phys. Chem.* **27**, 27 (2008).
5. Y. Marcus. *Ion Properties*, Marcel Dekker, New York (1997).
6. W. R. Fawcett. *J. Phys. Chem. B* **103**, 11181 (1999).
7. C. P. Kelly, C. J. Cramer, D. G. Truhlar. *J. Phys. Chem. B* **110**, 16066 (2006).
8. J. R. Pliego Jr., J. M. Riveros. *Phys. Chem. Chem. Phys.* **4**, 1622 (2002).
9. C. J. Cramer, D. G. Truhlar. *Chem. Rev.* **99**, 2161 (1999).
10. J. Tomasi, M. Persico. *Chem. Rev.* **94**, 2027 (1994).
11. S. Trasatti. *Pure App. Chem.* **58**, 955 (1986).

12. R. Parsons. In *Standard Potentials in Aqueous Solution*, A. J. Bard, R. Parsons, J. Jordan (Eds.), pp. 13–37, Marcel Dekker, New York (1985).
13. H. Reiss. *J. Electrochem. Soc.*, **C 135**, 247 (1988).
14. H. Reiss, A. Heller. *J. Phys. Chem.* **89**, 4207 (1985).
15. R. Gomer, G. Tryson. *J. Chem. Phys.* **66**, 4413 (1977).
16. W. N. Hansen, G. J. Hansen. *Phys. Rev. A* **36**, 1396 (1987).
17. W. N. Hansen, D. M. Kolb. *J. Electroanal. Chem.* **100**, 493 (1979).
18. H. Gerischer, W. Ekardt. *Appl. Phys. Lett.* **43**, 393 (1983).
19. E. Gileadi, G. Stoner. *J. Electroanal. Chem.* **36**, 492 (1972).
20. J. O. Bockris. *Energy Convers.* **10**, 41 (1970).
21. J. O. Bockris, S. D. Argade. *J. Chem. Phys.* **49**, 5133 (1968).
22. J. E. B. Randles. *Phys. Chem. Liq.* **7**, 107 (1977).
23. V. P. Sokhan, D. J. Tildesley. *Mol. Phys.* **92**, 625 (1997).
24. J. R. Farrell, P. McTigue. *J. Electroanal. Chem.* **139**, 37 (1982).
25. M. D. Tissandier, K. A. Cowen, W. Y. Feng, E. Gundlach, M. H. Cohen, A. D. Earhart, J. V. Coe, T. R. Tuttle Jr. *J. Phys. Chem. A* **102**, 7787 (1998).
26. T. R. Tuttle, Jr., S. Malaxos, J. V. Coe. *J. Phys. Chem. A* **106**, 925 (2002).
27. W. A. Donald, R. D. Leib, M. Demireva, J. T. O'Brien, J. S. Prell, E. R. Williams. *J. Am. Chem. Soc.* **131**, 13328 (2009).
28. W. A. Donald, R. D. Leib, J. T. O'Brien, M. F. Bush, E. R. Williams. *J. Am. Chem. Soc.* **130**, 3371 (2008).
29. W. A. Donald, R. D. Leib, J. T. O'Brien, E. R. Williams. *Chem.—Eur. J.* **15**, 5926 (2009).
30. W. A. Donald, E. R. Williams. *J. Phys. Chem. B* **114**, 13189 (2010).
31. V. S. Bryantsev, M. S. Diallo, W. A. Goddard III. *J. Phys. Chem. B* **112**, 9709 (2008).
32. C.-G. Zhan, D. A. Dixon. *J. Phys. Chem. A* **105**, 11534 (2001).
33. J. A. Mejías, S. Lago. *J. Chem. Phys.* **113**, 7306 (2000).
34. W. G. Madden, R. Gomer, M. J. Mandell. *J. Phys. Chem.* **81**, 2652 (1977).
35. Z. Samec, B. W. Johnson, K. Doblhofer. *Surf. Sci.* **264**, 440 (1992).
36. C. E. Klots. *J. Phys. Chem.* **85**, 3585 (1981).
37. J. V. Coe. *Chem. Phys. Lett.* **85**, 161 (1994).
38. W. A. Donald, E. R. Williams. *J. Am. Soc. Mass Spectrom.* **21**, 615 (2010).
39. W. A. Donald, M. Demireva, R. D. Leib, M. J. Aiken, E. R. Williams. *J. Am. Chem. Soc.* **132**, 4633 (2010).
40. W. A. Donald, R. D. Leib, J. T. O'Brien, A. I. S. Holm, E. R. Williams. *Proc. Natl. Acad. Sci. USA* **105**, 18102 (2008).
41. R. D. Leib, W. A. Donald, M. F. Bush, J. T. O'Brien, E. R. Williams. *J. Am. Chem. Soc.* **129**, 4894 (2007).
42. R. D. Leib, W. A. Donald, M. F. Bush, J. T. O'Brien, E. R. Williams. *J. Am. Soc. Mass Spectrom.* **18**, 1217 (2007).
43. R. D. Leib, W. A. Donald, J. T. O'Brien, M. F. Bush, E. R. Williams. *J. Am. Chem. Soc.* **129**, 7716 (2007).
44. J. S. Prell, J. T. O'Brien, A. I. S. Holm, R. D. Leib, W. A. Donald, E. R. Williams. *J. Am. Chem. Soc.* **130**, 12680 (2008).
45. J. T. O'Brien, J. S. Prell, A. I. S. Holm, E. R. Williams. *J. Am. Soc. Mass Spectrom.* **19**, 772 (2008).
46. P. Han, D. M. Bartels. *J. Phys. Chem.* **94**, 7294 (1990).
47. J. Jortner, R. M. Noyes. *J. Phys. Chem.* **70**, 770 (1966).
48. H. Shiraishi, G. R. Sunaryo, K. Ishigure. *J. Phys. Chem.* **98**, 5164 (1994).
49. H. A. Schwarz. *J. Phys. Chem.* **95**, 6697 (1991).

50. W. A. Donald, R. D. Leib, M. Demireva, B. Negru, D. M. Neumark, E. R. Williams. *J. Phys. Chem. A* **115**, 2 (2011).
51. H. I. Kenttamaa, R. G. Cooks. *Int. J. Mass Spectrom. Ion Processes* **64**, 79 (1985).
52. W. A. Donald, R. D. Leib, M. Demireva, B. Negru, D. M. Neumark, E. R. Williams. *J. Am. Chem. Soc.* **132**, 6904 (2010).
53. A. I. S. Holm, W. A. Donald, P. Hvelplund, M. K. Larsen, S. B. Nielsen, E. R. Williams. *J. Phys. Chem. A* **112**, 10721 (2008).
54. M. Demireva, E. R. Williams. *J. Am. Soc. Mass Spectrom.* **21**, 1133 (2010).
55. R. F. Höckendorf, O. P. Balaj, C. van der Linde, M. K. Beyer. *Phys. Chem. Chem. Phys.* **12**, 3772 (2010).
56. M. Demireva, E. R. Williams. (2011). Manuscript in preparation.
57. M. F. Bush, R. J. Saykally, E. R. Williams. *Int. J. Mass Spectrom.* **253**, 256 (2006).
58. R. L. Wong, K. Paech, E. R. Williams. *Int. J. Mass Spectrom.* **232**, 59 (2004).
59. R. B. Cody, R. E. Hein, S. D. Goodman, A. G. Marshall. *Rapid Commun. Mass Spectrom.* **1**, 99 (1987).
60. N. G. Adams, V. Poterya, L. M. Babcock. *Mass Spectrom. Rev.* **25**, 798 (2006).
61. A. Al-Khalili, R. Thomas, A. Ehlerding, F. Hellberg, W. D. Geppert, V. Zhaunerchyk, E. Uggerud, J. Vedde, C. Adlhart, J. Semaniak, M. Kamińska, R. A. Zubarev, F. Kjeldsen, P. U. Andersson, F. Österdahl, V. A. Bednarska, A. Paál. *J. Chem. Phys.* **121**, 5700 (2004).
62. V. Zhaunerchyk, A. Ehlerding, W. D. Geppert, F. Hellberg, R. D. Thomas, M. Larsson, A. A. Viggiano, S. T. Arnold, F. Österdahl, P. Hlavenka. *J. Chem. Phys.* **121**, 10483 (2004).
63. M. B. Någård, J. B. C. Pettersson, A. M. Derkatch, A. Al Khalili, A. Neau, S. Rosén, M. Larsson, J. Semaniak, H. Danared, A. Källberg, F. Österdahl, M. Af Ugglas. *J. Chem. Phys.* **117**, 5264 (2002).
64. A. Neau, A. Al Khalili, S. Rosén, A. Le Padellec, A. M. Derkatch, W. Shi, L. Viktor, M. Larsson, J. Semaniak, R. Thomas, M. B. Någård, K. Andersson, H. Danared, M. Af Ugglas. *J. Chem. Phys.* **113**, 1762 (2000).
65. J. S. Prell, J. T. O'Brien, E. R. Williams. *J. Am. Soc. Mass Spectrom.* **21**, 800 (2010).
66. D. R. Lide (Ed.). *CRC Handbook of Chemistry and Physics, Internet Version*, Taylor and Francis, Boca Raton, FL (2007).
67. F. Chen, E. R. Davidson. *J. Phys. Chem. A* **105**, 10915 (2001).
68. D. M. Hudgins, R. F. Porter. *Int. J. Mass Spectrom. Ion Proc.* **130**, 49 (1994).
69. A. L. Sobolewski, W. Domcke. *Phys. Chem. Chem. Phys.* **9**, 3818 (2007).
70. Y. Itikawa, N. Mason. *J. Phys. Chem. Ref. Data* **34**, 1 (2005).
71. D. Neff, J. Simons. *Int. J. Mass Spectrom.* **277**, 166 (2008).
72. C. E. Klots. *J. Chem. Phys.* **83**, 5854 (1985).
73. W. A. Donald, E. R. Williams. *J. Phys. Chem. A* **112**, 3515 (2008).
74. P. M. Holland, A. W. Castleman Jr. *J. Phys. Chem.* **86**, 4181 (1982).
75. M. Born. *Z. Physik* **1**, 45 (1920).
76. J. Gulens, J. A. Page. *J. Electroanal. Chem.* **67**, 215 (1976).
77. N. J. Curtis, G. A. Lawrance, A. M. Sargeson. *Aust. J. Chem.* **36**, 1327 (1983).
78. E. L. Yee, R. J. Cave, K. L. Guyer, P. D. Tyma, M. J. Weaver. *J. Am. Chem. Soc.* **101**, 1131 (1979).
79. M. J. Weaver, P. D. Tyma, S. M. Nettles. *J. Electroanal. Chem.* **114**, 53 (1980).
80. A. J. Bard, L. R. Faulkner. *Electrochemical Methods: Fundamentals and Applications*, 2nd ed., John Wiley, New York (2001).
81. G. Milazzo, S. Caroli, V. K. Sharma. *Tables of Standard Electrode Potentials*, John Wiley, Chichester (1978).
82. C. F. Baes. *The Hydrolysis of Cations*, John Wiley, New York (1976).
83. D. R. Lide (Ed.). *CRC Handbook of Chemistry and Physics, Internet Version*, Taylor and Francis, Boca Raton, FL (2007).

84. M. F. Bush, R. J. Saykally, E. R. Williams. *Chem. Phys. Chem.* **8**, 2245 (2007).
85. M. F. Bush, R. J. Saykally, E. R. Williams. *J. Am. Chem. Soc.* **130**, 15482 (2008).
86. M. F. Bush, J. T. O'Brien, J. S. Prell, C. C. Wu, R. J. Saykally, E. R. Williams. *J. Am. Chem. Soc.* **131**, 13270 (2009).
87. M. F. Bush, R. J. Saykally, E. R. Williams. *J. Am. Chem. Soc.* **130**, 9122 (2008).
88. J. S. Prell, J. T. O'Brien, E. R. Williams. *J. Am. Chem. Soc.* **133**, 4810 (2011).
89. J. T. O'Brien, J. S. Prell, M. F. Bush, E. R. Williams. *J. Am. Chem. Soc.* **132**, 8248 (2010).
90. J.-W. Shin, N. I. Hammer, E. G. Diken, M. A. Johnson, R. S. Walters, T. D. Jaeger, M. A. Duncan, R. A. Christie, K. D. Jordan. *Science* **304**, 1137 (2004).
91. M. Miyazaki, A. Fujii, T. Ebata, N. Mikami. *Science* **304**, 1134 (2004).
92. R. S. Walters, E. D. Pillai, M. A. Duncan. *J. Am. Chem. Soc.* **127**, 16599 (2005).
93. S. Gopalakrishnan, D. Liu, H. C. Allen. *Chem. Rev.* **106**, 1155 (2006).
94. M. J. Shultz, C. Schnitzer, D. Simonelli, S. Baldelli. *Int. Rev. Phys. Chem.* **19**, 123 (2000).
95. Y. R. Shen, V. Ostroverkhov. *Chem. Rev.* **106**, 1140 (2006).
96. G. L. Richmond. *Chem. Rev.* **102**, 2693 (2002).
97. N. Ji, V. Ostroverkhov, C. S. Tian, Y. R. Shen. *Phys. Rev. Lett.* **100**, 096102 (2008).
98. M. Peschke, A. T. Blades, P. Kebarle. *J. Phys. Chem. A* **102**, 9978 (1998).
99. S. E. Rodriguez-Cruz, R. A. Jockusch, E. R. Williams. *J. Am. Chem. Soc.* **120**, 5842 (1998).
100. S. E. Rodriguez-Cruz, R. A. Jockusch, E. R. Williams. *J. Am. Chem. Soc.* **121**, 8898 (1999).
101. D. R. Carl, R. M. Moision, P. B. Armentrout. *Int. J. Mass Spectrom.* **265**, 308 (2007).
102. M. Pavlov, P. E. M. Siegbahn, M. Sandström. *J. Phys. Chem. A* **102**, 219 (1998).
103. J. E. B. Randles. *Phys. Chem. Liq.* **7**, 107 (1977).
104. T. Frigato, J. VandeVondele, B. Schmidt, C. Schutte, P. Jungwirth. *J. Phys. Chem. A* **112**, 6125 (2008).
105. G. Makov, A. Nitzan. *J. Phys. Chem.* **98**, 3459 (1994).